New modulated design and synthesis of quercetin–CuII/Zn II–Sn2IV scaffold as anticancer agents: In vitro DNA binding profile, DNA cleavage pathway and Topo–I activity

ARTICLE *in* DALTON TRANSACTIONS · MAY 2013

Impact Factor: 4.2 · DOI: 10.1039/c3dt50646k · Source: PubMed

4 AUTHORS, INCLUDING:

Mohd Afzal
North Eastern Regional Institute of Science …
25 PUBLICATIONS **267** CITATIONS
SEE PROFILE

Farukh Arjmand
Aligarh Muslim University
111 PUBLICATIONS **1,359** CITATIONS
SEE PROFILE

Dalton Transactions

RSC Publishing

PAPER

View Article Online
View Journal | View Issue

Cite this: *Dalton Trans.*, 2013, **42**, 10029

New modulated design and synthesis of quercetin–Cu^{II}/Zn^{II}–Sn_2^{IV} scaffold as anticancer agents: *in vitro* DNA binding profile, DNA cleavage pathway and Topo-I activity†

Sartaj Tabassum,* Mehvash Zaki, Mohd. Afzal and Farukh Arjmand

New molecular topologies quercetin–Cu^{II}–Sn_2^{IV} and Zn^{II}–Sn_2^{IV} **1** and **2** were designed and synthesized to act as potential cancer chemotherapeutic agents. Their interaction with CT DNA by UV-vis and fluorescence spectroscopy was evaluated revealing an electrostatic mode of binding. Quercetin complexes are capable of promoting DNA cleavage involving both single and double strand breaks. Complex **1** cleaved pBR322 DNA *via* an oxidative mechanism while **2** followed a hydrolytic pathway, accessible to the minor groove of the DNA double helix in accordance with molecular docking studies with the DNA duplex of sequence $d(CGCGAATTCGCG)_2$ dodecamer demonstrating that the complex was stabilized by additional electrostatic and hydrogen bonding interactions with the DNA. ROS such as $OH^{\cdot}$, H_2O_2 and $O_2^{\cdot -}$ are the major metabolites responsible for chronic diseases such as cancer, respiratory disorders, HIV, and diabetes *etc.*, therefore eliminating ROS by molecular scaffolds involving SOD enzymatic activity has emerged as a potential way to develop a novel class of drugs. Therefore, *in vitro* superoxide dismutase activity of redox active complex **1** was evaluated by using a xanthine/xanthine oxidase-NBT assay which showed an IC_{50} value of 2.26 μM. Moreover, the cytotoxicity of both the complexes were screened on a panel of human carcinoma cell lines (GI_{50} values <8.7 μM) which revealed that **1** has a better prospect of acting as a cancer chemotherapeutic agent, and to elucidate the mechanism of tumor inhibition, Topo-I enzymatic activity was carried out. Furthermore, molecular modeling studies were carried out to understand molecular features important for drug–enzyme interactions which offer new insights into the experimental model observations.

Received 8th March 2013,
Accepted 11th April 2013

DOI: 10.1039/c3dt50646k

www.rsc.org/dalton

Introduction

Metal-based cancer drugs are widely used clinically and have attracted much attention after the successful development of cisplatin and its rapid utilization in combination regimens for a variety of other carcinomas, including bladder, small cell lung and head and neck cancers and against small-cell lung cancer with a cure rate as high as 90%.[1] However, its clinical utility is limited regarding its toxicity issues such as intrinsic resistance to a relatively narrow range of tumors, because of primary resistance to cisplatin.[2,3] Therefore an appropriate choice of metals in a pharmacologically active organic scaffold changes the pharmacological activity and literature reveals that the pharmacological activity depends on the metal ion and organic scaffold and specific DNA binding site.[3]

DNA is generally the primary intracellular target of anticancer drugs, so the interaction between small molecules and DNA can cause DNA damage in cancer cells, blocking the division of cancer cells, and resulting in cell death.[4,5] Small molecules can interact with DNA through the following three noncovalent modes: intercalation, groove binding, and external static electronic effects.[6] Recently, there has been great interest on the binding of transition metal complexes with DNA, owing to their possible applications as new cancer therapeutic agents.[7–9] It has been demonstrated that copper accumulates in tumors due to selective permeability of the cancer cell membrane to copper compounds thereby they can act as "artificial nucleases" for the sequence specific disruption of gene function. While zinc as an essential element plays a vital role in many physiological, and pathological processes. Zinc controls cell proliferation, differentiation, and viability including

Department of Chemistry, Aligarh Muslim University, Aligarh, UP-202002, India. E-mail: tsartaj62@yahoo.com; Tel: +91 9358255791

†Electronic supplementary information (ESI) available: Spectroscopic and analytical techniques for the characterization of complexes and DNA binding studies. See DOI: 10.1039/c3dt50646k

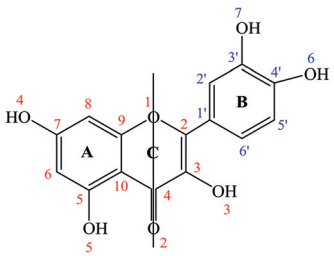

Fig. 1 Molecular structure of quercetin.

apoptosis. On the other hand tin complexes show preferential selectivity towards the oxygen atom of the polyanionic structure of DNA, Sn^{IV} ions possess a hard Lewis acid nature, and interact with the phosphate backbone and thus bring about conformational changes in DNA. We have demonstrated earlier in our previous studies that heterobimetallic complexes of Cu^{II}–Sn^{IV} exhibit a remarkable antiproliferative profile and show preferential selectivity inside the cells, inducing apoptosis *via* the mitochondrial pathway.[10,11] Thus, heterobimetallic complexes containing Cu^{II}/Zn^{II} and Sn^{IV} ions enhance the chemotherapeutic action many-fold as they provide a dual mode of binding at the molecular target site and also exhibit novelty due to preferential selectivity inside the cells.[12] The interaction of metal complexes of flavonoids notably quercetin (Fig. 1) with DNA exhibits biochemical and biological importance, such as anticancer, antiviral, antibacterial, antioxidants, and anti-inflammatory effects. DNA–quercetin interaction has been studied intensively, since these molecules exhibited a high potential to act as chemotherapeutic agents, mainly in cancer chemotherapy. Topoisomerases are one of the major targets in anti-cancer drug development because they can cause permanent DNA damage and can lead to cell cycle arrest and/or cell death by apoptosis. Literature revealed that selective DNA–Topo-I inhibitors such as camptothecin (anticancer drug), Hoechst 33258 and bleomycin have been approved as antineoplastic and antiproliferative agents.[13] In order to develop efficient metal-based therapeutic molecular entities for the treatment of cancer, herein we report synthetic design and DNA binding profile of heterobimetallic Cu^{II}/Zn^{II}–Sn_2^{IV} complexes as topoisomerase I inhibitor. *In vitro* DNA binding and cleavage studies revealed that these complexes are avid DNA binding agents and act as potent Topo-I inhibitors. In addition, the superoxide dismutase activity of complex **1** showed excellent SOD mimic characteristics by catalyzing the disproportionation of the superoxide anion into oxygen and hydrogen peroxide under physiological conditions.

Results and discussion

New heterobimetallic quercetin–Cu^{II}–Sn_2^{IV} and Zn^{II}–Sn_2^{IV} complexes (**1** and **2**) were designed and synthesized (Scheme 1). The complexes are stable towards air and soluble in methanol and DMSO. The complexes were thoroughly characterized from analytical and physicochemical data. Molar conductance values of all the complexes in DMSO (1×10^{-3} M) at 25 °C were too low to account for any dissociative ions in the complexes, indicating the non-electrolytic nature of complexes. The complexes **1** and **2** revealed octahedral coordination geometry for the central metal ions Cu^{II}/Zn^{II} as well as for the Sn^{IV} ions as proposed by various spectroscopic studies.

IR spectra

The IR spectra of heterobimetallic complexes **1** and **2** displayed characteristic broad bands at 3392–3463 cm^{-1} merged with the ν(O–H) stretching vibration of coordinated water molecules and OH groups of quercetin. Specifically in free quercetin, the ν(C=O) band around 1667 cm^{-1} was shifted to lower frequencies in heterobimetallic complexes (1620–1644 cm^{-1}) suggesting the coordination of quercetin *via* the oxygen atom of carbonyl group. However, a band at 1270–1274 cm^{-1} assigned to ν(C–O–C) stretching frequency in complexes remained unaffected indicating that the ring oxygen atom was not involved in the complexation.[14] In addition the formation of complexes were affirmed by the presence of medium

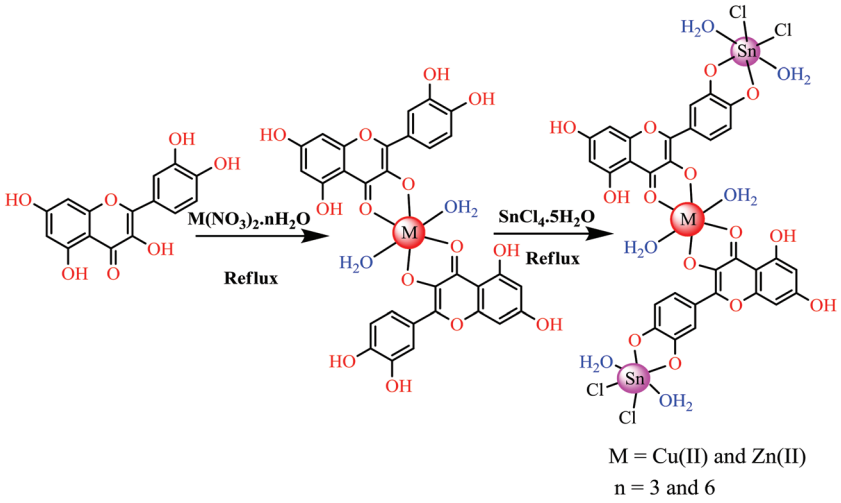

Scheme 1 Synthetic route to monometallic and heterobimetallic complexes.

intensity bands around 651–655 and 404–416 cm^{-1} attributed to the ν(Cu/Zn–O) and ν(Sn–O) vibrations, respectively.[15,16]

NMR spectral studies

The NMR spectrum of heterobimetallic complex **2** was recorded in DMSO-d_6 solution. ^1H NMR spectrum did not show any resonance signals for the free 3′-OH and 4′-OH groups which is commensurate with the fact that the –OH proton was coordinated simultaneously to Sn^{IV} metal ion through deprotonation. However, the signals at 10.68 and 12.59 ppm were attributed to the presence of 7-OH and 5-OH groups in the complex.[15] The resonance signal at 3.6 ppm was consistent with the presence of coordinated H_2O molecules in complexes. The aromatic protons of the quercetin ring appeared as multiplets in the range of 6.2–7.4 ppm.[17]

The ^{13}C NMR spectrum displayed characteristic resonance signals of aromatic rings in the 118–155 ppm range, whereas the carbon atoms attached to the –OH groups were observed slightly upfield in the 139–164 ppm range. However, a prominent resonance peak for the carbonyl group was observed at 175 ppm.[18]

The ^{119}Sn NMR spectrum exhibited two signals at −541 and −546 ppm, due to the presence of two Sn metal centers consistent with the octahedral geometry around the Sn(IV) ion (Fig. S1†).[19]

Mass spectra

The ESI mass spectra of heterobimetallic complexes **1** and **2** exhibited peaks at *m*/*z* 1113.6 and 1115.5 assigned to and $[C_{30}H_{26}Cl_4O_{20}Sn_2Cu–2H_2O]^+$ $[C_{30}H_{26}Cl_4O_{20}Sn_2Zn–2H_2O]^+$ fragments, respectively. The appearance of other prominent peaks for complex **1** at *m*/*z* 1079.3, 1040.3 and 660.5 correspond to the fragments $[C_{30}H_{26}Cl_4O_{20}Sn_2Cu–4H_2O–3H]^+$, $[C_{30}H_{26}Cl_4O_{20}Sn_2Cu–6H_2O]^+$ and $[C_{30}H_{26}Cl_4O_{20}Sn_2Cu–6H_2O–2SnCl_2 + 5H]^+$, respectively. Similarly for complex **2** peaks at *m*/*z* 1080.3, 1040.7 and 667.8 were assigned to $[C_{30}H_{26}Cl_4O_{20}Sn_2Zn–4H_2O + 3H]^+$, $[C_{30}H_{26}Cl_4O_{20}Sn_2Zn–6H_2O + H]^+$ and $[C_{30}H_{26}Cl_4O_{20}Sn_2Zn–6H_2O–2SnCl_2–H]^+$ fragments, respectively (Fig. S2†).

Thermal analysis

To determine the thermal stability of complexes, thermogravimetric analysis was performed under a nitrogen atmosphere in the temperature range 20–1000 °C at a heating rate of 20 °C min^{-1}. The TGA curves of complexes indicated the weight loss in 3 steps: over the temperature range 160–170, 430–590 and 874–887 °C (Fig. S3†). The first step revealed the simultaneous degradation of six water molecules and four chloride ions in the temperature range 160–170 °C accompanied by a net weight loss of 27.22 and 24.64% (calculated: 23.15 and 23.19%), respectively. In the second step, as the temperature increased, further weight loss of 70.32 and 73.41% (calculated: 72.63 and 72.79%) was observed gradually, which was attributed to the pyrolysis of two quercetin molecules in the temperature range 430–590 °C. Finally, at 874–887 °C a total weight loss occurred leading to the formation of metal oxides.

EPR spectra

The liquid state X-band EPR spectrum of complex **1** was recorded in DMSO at liquid nitrogen temperature on X-band at frequency of 9.1 GHz under the magnetic field strength of 3000 G as shown in Fig. S4.† The EPR spectrum revealed an anisotropic signal with $g_\parallel = 2.15$, $g_\perp = 2.03$ and $g_{av} = 2.07$ computed from the expression $g_{av}^2 = (g_\parallel^2 - g_\perp^2)/3$. The ordering of *g* values $g_\parallel > g_\perp > 2.0023$ for **1** revealed that the unpaired electron most likely localized in the $d_{x^2-y^2}$ orbital of the Cu^{II} ion consistent with a tetragonally elongated octahedral geometry.[20] Furthermore the exchange interaction parameter $G > 4$ (5.0), indicates that there is no exchange interaction between the copper centers and the local tetragonal axis are aligned parallel or slightly misaligned with an unpaired electron in the $d_{x^2-y^2}$ orbital. For a copper complex the $g_\parallel$ parameter is sensitive enough to indicate covalence.[21] For a covalent Cu^{II} complex $g_\parallel < 2.3$ and for an ionic environment, normally $g_\parallel$ = 2.3 or more. The *g* values obtained for this complex were found to be less than 2.3 consistent with metal ligand covalent character.

Electronic spectra

The UV-vis spectra of heterobimetallic complexes **1** and **2** were recorded in DMSO at room temperature. The electronic spectra of complexes exhibited two absorption bands in the range 273–275 (ε = 800–1200 L mol^{-1} cm^{-1}) and 430–462 nm (ε = 700–800 L mol^{-1} cm^{-1}) due to the intraligand transitions of the cinnamoyl and benzoyl system of quercetin, respectively.[22] Furthermore, the complex **1** displayed a broad absorption band at 797 nm (ε = 500 L mol^{-1} cm^{-1}) attributed to the $^2E_g \rightarrow {}^2T_{2g}$ transition. This spectral feature is typical for octahedral geometry of Cu^{II} ion in complex **1**.[23]

DNA binding studies

Electronic absorption titration. The interaction of transition metal complexes with DNA takes place *via* both covalent and/or non-covalent interactions. In the case of covalent binding, the labile ligand of the complexes is replaced by a nitrogen base of DNA such as guanine N7 while the non-covalent DNA interactions include intercalative, electrostatic and groove binding of metal complexes outside of a DNA helix. The absorption spectra of complexes **1** and **2** exhibited hyperchromism of 31.57% and 23.68%, respectively at intraligand absorption band (267–271 nm) as depicted in Fig. S5.† The observed hyperchromic effect revealed that complexes **1** and **2** bind to DNA electrostatically *via* external contact with the DNA duplex. Moreover, complexes **1** and **2** exhibited a higher DNA binding profile due to the incorporation of Sn^{IV} ions in the monometallic core; Sn^{IV} ions possess a hard Lewis acid nature and selectively bind to the phosphate backbone of a DNA helix.[24] Furthermore, the presence of transition metal ions Cu^{II}/Zn^{II} in complexes prefer coordinate covalent binding to N7/N3 of nucleobases and expose the embedded base pairs to the helix exterior ultimately leading to strand breakage.[25] Since complexes **1** and **2** possess the heterobimetallic core

Cu^{II}–Sn_2^{IV}/Zn^{II}–Sn_2^{IV} they therefore exhibited a dual mode of preferential binding that is electrostatic interaction by Sn(IV) ions preferentially towards the oxygen atoms of vicinal phosphate moiety reinstated further by coordinate covalent binding of Cu^{II}/Zn^{II} ion to N7/N3 atom of nucleobases. Moreover, the hydrogen bonding interactions between –OH groups of quercetin and the functional groups positioned on the edge of DNA bases feature novelty as it provides molecular recognition at the specific site at the cellular target. The intrinsic binding constant values (K_b) of the complexes were determined by monitoring the changes in the absorbance at the intraligand band with increasing concentration of CT DNA (Table S1†). The binding constants obtained for complexes **1** and **2** are 6.7×10^5 and 3.5×10^5 M^{-1}, respectively. Interestingly, the intrinsic binding K_b value of complex **1** was much higher in magnitude in comparison to our previous Cu^{II}–Sn^{IV} heterobimetallic complex (K_b value 3.0×10^4 M^{-1}) which demonstrates the remarkably higher binding propensity of complex **1** towards DNA.[24]

Fluorescence spectral studies. The emission spectra of complex **1** and **2** displayed an intense luminescence at 336 nm in 0.01 Tris-HCl/50 mM NaCl buffer at room temperature when excited at 269 nm. On addition of increasing concentration of CT DNA (0.70×10^{-5} to 4.24×10^{-5} M) to a fixed amount of complexes, the emission intensity gradually increases with no apparent change in the shape and position of the emission bands as shown in Fig. S6.† The enhancement in emission intensity is related to the extent to which the complex penetrates into the hydrophobic environment inside the DNA helix therefore complex mobility is restricted at the binding site leading to a decrease in the vibrational mode of relaxation and thus avoids the quenching effect of the solvent molecules. The increase in emission intensity revealed that the complex interacts by hydrophobic interaction in the DNA major and minor grooves.[26] The binding constant determined from the Scatchard equation for complexes **1** and **2** was calculated to be 6.18×10^5 and 4.33×10^5 M^{-1}, respectively.

Effect of $K_4[Fe(CN)_6]$. The steady state emission quenching experiments using $K_4[Fe(CN)_6]$ as a quencher were performed to examine the binding of complexes to CT DNA. $[Fe(CN)_6]^{4-}$ is a dynamic fluorescence quencher and provides a sensitive tool to examine the nature of interaction of complexes with CT DNA. $[Fe(CN)_6]^{4-}$ poorly quench the fluorescence intensity of complexes that strongly bind to the DNA since the complexes are efficiently protected by the DNA helix whereas the complexes which are free in solution are quenched due to ion pairing.[27] The quenching efficiency was evaluated by using the Stern–Volmer equation. Addition of anionic quencher greatly affects the emission intensities of complexes **1** and **2**. The decrease in the emission intensities of the complexes were due to the repulsion between the highly negatively charged $[Fe(CN)_6]^{4-}$ and negatively bound DNA phosphate backbone, which hinders access of $[Fe(CN)_6]^{4-}$ to the DNA-bound complexes. The plots of free complexes gave K_{sv} value of 1.95×10^5 and 1.42×10^5 respectively. In the presence of DNA the quenching curve was depressed (Fig. S7†) due to the protection of complexes by the DNA helix and the K_{sv} value of complexes **1** and **2** decreased to 1.07×10^5 and 1.19×10^5 respectively.[28] The greater decrease in the K_{sv} value of **1** as compared to **2** signifies the high DNA binding propensity of **1**.

Ethidium bromide displacement assay. To further clarify the mode of binding of complexes **1** and **2** competitive ethidium bromide displacement assay was carried out. The extent of quenching of the fluorescence of DNA bound EB would reflect the extent of DNA binding of complexes **1** and **2** (Fig. S8†). EB is a phenanthridine fluorescence dye, a typical indicator of intercalation since it forms soluble complexes with nucleic acids emitting intense fluorescence when intercalated into the base pairs of DNA.[29] The addition of a second DNA-binding molecule can quench the emission intensity of DNA–EB system by either replacing the EB and/or by accepting the excited-state electron of the EB through a photoelectron transfer mechanism.[30] The decrease in emission intensity is due to the displacement of EB from DNA–EB system by complex molecules, suggesting its strong competition for the intercalative binding site. Since EB was not completely displaced, partial intercalation in addition to the electrostatic mode of binding cannot be ruled out. Furthermore, the quenching extent was evaluated quantitatively by employing the Stern–Volmer equation. The K_{sv} value for complexes **1** and **2** were found to be 0.44 and 0.031, respectively. The corroborative results of *in vitro* DNA binding experiments of the complexes reveal that complex **1** is an outstanding drug candidate for cancer chemotherapy.

DNA cleavage activity

DNA cleavage without adding reductant. In order to ascertain the DNA cleavage ability of complexes **1** and **2**, supercoiled pBR322 DNA was incubated with increasing concentration of complex in 5 mM Tris-HCl/40 mM NaCl buffer solution (pH 7.42) for 45 min without addition of any reductant. The activity of complex **1** and **2** was assessed by the conversion of pBR322 DNA from Form I (supercoiled form) to Form II (nicked circular) and then to Form III (linear form). The concentration dependent DNA cleavage activity of complex **1** and **2** was observed by gel electrophoresis (Fig. 2). With increase in concentration of complex **1** and **2**, the amount of Form I of

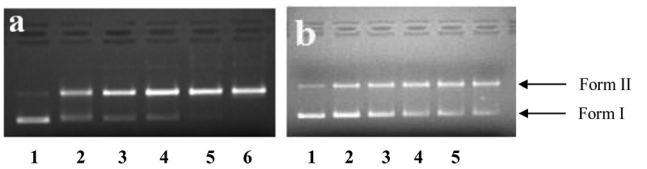

Fig. 2 Agarose gel electrophoresis pattern for the cleavage of pBR322 plasmid DNA (300 ng) by complexes **1** and **2** at 37 °C after incubation for 45 min (a) at different concentrations of **1**; lane 1: DNA control; lane 2: 5 μM complex **1** + DNA; lane 3: 10 μM complex **1** + DNA; lane 4: 15 μM complex **1** + DNA; lane 5: 20 μM complex **1** + DNA; lane 6: 25 μM complex **1** + DNA. (b) At different concentrations of **2**; lane 1: DNA control; lane 2: 5 μM complex **2** + DNA; lane 3: 10 μM complex **2** + DNA; lane 4: 15 μM complex **2** + DNA; lane 5: 20 μM complex **2** + DNA; lane 6: 25 μM complex **2** + DNA.

pBR322 DNA gradually diminishes whereas Form II increases, suggesting the single strand DNA cleavage.[31] At 25 μM concentration, complexes exhibited efficient nuclease activity, the supercoiled form (Form I) relaxes to generate nicked form (Form II). However, in the case of complex **1** there was a complete conversion of Form I into Form II which reveals a higher cleavage efficiency of complex **1** in comparison to complex **2**; with an increase in concentration, an intensified nicked form (Form II) was observed. From the cleavage patterns it was clearly observed that the intensity of Form II of DNA was higher in complex **1** than complex **2**, which corroborated well with the DNA binding studies.

DNA cleavage in the presence of activators. The nuclease efficiency of metal complexes sometimes depends on the activators used for initiating the DNA cleavage process. Therefore, the DNA cleavage activity of complexes **1** and **2** was evaluated in the presence and absence of activators *viz.*; H_2O_2, ascorbate, 3-mercaptopropionic acid and glutathione as shown in Fig. 3. The results revealed that the cleavage activity of complexes was significantly enhanced in the presence of these activators and follows the order H_2O_2 > MPA > GSH > Asc for complex **1** and H_2O_2 > MPA > GSH ≈ Asc for complex **2**. The complex **1** in the presence of H_2O_2 exhibited significant DNA cleavage activity, followed by complete degradation of DNA was observed.

DNA cleavage in the presence of reactive oxygen species. In order to investigate the role of reactive oxygen species which was responsible for the DNA cleavage mediated by complex **1** and **2**, reactions were carried out in the presence of hydroxyl radical scavengers (DMSO and EtOH), singlet oxygen quencher (NaN_3) and superoxide oxygen scavenger (SOD) under identical conditions. As shown in Fig. 4, the DMSO and EtOH scarcely inhibited the DNA cleavage (lanes 2 and 3) suggestive of non-involvement of diffusible hydroxyl radical as one of the reactive species involved in the cleavage process. On the other hand addition of NaN_3 and SOD (lanes 4 and 5) showed little inhibitory effect on the DNA cleavage. However, H_2O_2 could markedly promote the strand breakage of plasmid pBR322 DNA induced by the complex (lane 3, Fig. 4a), as indicated by the appearance of linear Form III. This indicates that hydrogen peroxide plays a role to aid the complexes in DNA degradation by oxidative cleavage, and engages in an oxidation reaction on the DNA strand. Furthermore, Cu^{II} complex in equilibrium with the Cu^{I} complex takes one electron from the hydroxo oxygen and is converted into quercetin radical (Que˙), subsequently reacts with H_2O_2 to generate the DNA–Cu(I)OOH peroxide complex. Thereafter, the reduction of DNA–Cu(I)OOH peroxide complex generates ROS in bulk and produces more chain breaks in the proximity of DNA in a similar way to that of nuclease.[32]

In the case of complex **2** significant inhibition of the DNA cleavage activity was observed in the presence of DMSO and ethanol suggesting the possibility of hydroxyl radicals as one of the active species. On the other hand, NaN_3 has no significant effect which demonstrates that singlet oxygen was hardly involved in the DNA cleavage. However, addition of superoxide dismutase SOD (lane 9) enhances the cleavage efficiency in complex **2**, and displayed concomitant conversion of Form II to Form III. Therefore, an oxidative cleavage pathway of DNA by complex **2** has been excluded and evidently the cleavage proceeds by a hydrolytic mechanism. Since, complex **2** contains a coordinated water molecule, which facilitates the nucleophilic attack of water oxygen to phosphorus to give a five-coordinate phosphate intermediate and subsequent rearrangement of the phosphate, which allows the DNA to be

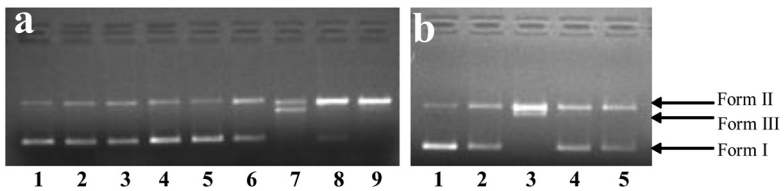

Fig. 3 Agarose gel electrophoresis pattern for the cleavage pattern of pBR322 DNA (300 ng) by complexes **1** and **2** at 37 C after incubation for 45 min (30 μM). (a) In absence and presence of complex **1** with different activating agents; lane 1, DNA control; lane 2, DNA + Asc (0.4 mM); lane 3, DNA + H_2O_2 (0.4 mM); lane 4, DNA + GSH (0.4 mM); lane 5, DNA + MPA (0.4 mM); lane 6, DNA + **1** + Asc (0.4 mM); lane 7, DNA + **1** + H_2O_2 (0.4 mM); lane 8, DNA + **1** + GSH (0.4 mM); lane 9, DNA + **1** + MPA (0.4 mM). (b) In the presence of complex **2** with different activating agents; lane 1, DNA control; lane 2, DNA + **2** + Asc (0.4 mM); lane 3, DNA + **2** + H_2O_2 (0.4 mM); lane 4, DNA + **2** + GSH (0.4 mM); lane 5, DNA + **2** + MPA (0.4 mM).

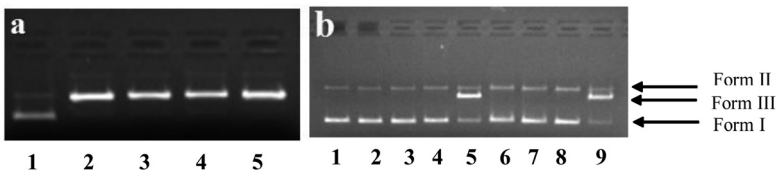

Fig. 4 Agarose gel electrophoresis pattern for the cleavage pattern of pBR322 DNA (300 ng) by complex **1** and **2** at 37 C after incubation for 45 min (30 μM). (a) In the presence of complex **1** with different radical scavengers; lane 1, DNA control; lane 2, DNA + **1** + DMSO (0.4 mM); lane 3, DNA + **1** + EtOH (0.4 mM); lane 4, DNA + **1** + NaN_3 (0.4 mM); lane 5, DNA + **1** + SOD (0.25 mM). (b) In the absence and presence of complex **2** with different radical scavengers; lane 1, DNA control; lane 2, DNA + DMSO (0.4 mM); lane 3, DNA + EtOH (0.4 mM); lane 4, DNA + NaN_3 (0.4 mM); lane 5, DNA + SOD (0.25 mM); lane 6, DNA + **2** + DMSO (0.4 mM); lane 7, DNA + **2** + EtOH (0.4 mM); lane 8, DNA + **2** + NaN_3 (0.4 mM); lane 9, DNA + **2** + SOD (0.25 mM).

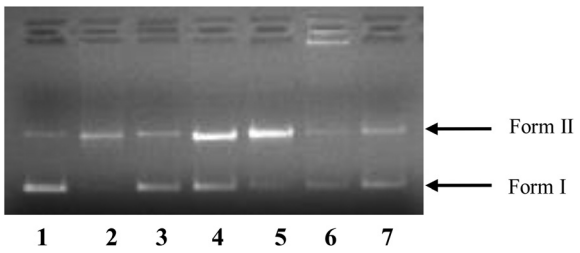

Fig. 5 Agarose gel electrophoresis pattern for the cleavage of pBR322 plasmid DNA (300 ng) by complexes **1** and **2** at 37 °C after incubation for 45 min in the presence of DNA minor groove binding agent DAPI and major groove binding agent methyl green; lane 1, DNA control; lane 2, DNA + DAPI (8 μM); lane 3, DNA + methyl green (2.5 μL of a 0.01 mg ml^{-1} solution); lane 4, DNA + **1** + DAPI (8 μM); lane 5, DNA + **1** + methyl green (2.5 μL of a 0.01 mg ml^{-1} solution); lane 6, DNA + **2** + DAPI (8 μM); lane 7, DNA + **2** + methyl green (2.5 μL of a 0.01 mg ml^{-1} solution).

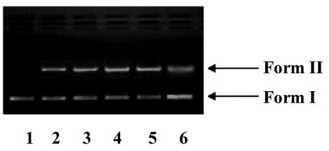

Fig. 6 Agarose gel electrophoresis patterns showing the effect of different concentrations of complex **1** on the activity of DNA topoisomerase I (Topo-I); lane 1, DNA control; lane 2, Topo-I + DNA; lane 3, 15 μM complex **1** + DNA + Topo-I; lane 4: 20 μM complex **1** + DNA + Topo-I; lane 5: 25 μM complex **1** + DNA + Topo-I; lane 6: 30 μM complex **1** + DNA + Topo-I.

cleaved readily. These results are consistent with the literature which reveals that Zn^{II} complexes generally cleave the DNA by a hydrolytic pathway (Fig. 4b).

DNA cleavage in the presence of recognition elements. Minor groove binding agent DAPI and major groove binding agent methyl green were used to probe the potential interacting site of complexes **1** and **2** with supercoiled plasmid pBR322 DNA. As shown in Fig. 5, DNA cleavage activity was strongly inhibited in the presence of DAPI in both the complexes. However, no apparent inhibition of DNA damage was observed with methyl green in the presence of complex **1** while in the case of complex **2** DNA cleavage remained unaffected, in the presence and absence of complex **2** suggesting the minor groove binding of both the complexes.

Topoisomerase I inhibition. A standard plasmid cleavage assay was used to investigate the effect of complex **1** on the activity of human Topo-I by agarose gel electrophoresis. This assay provides a direct means of determining whether the complex affects the unwinding of a supercoiled (SC) duplex DNA to nicked open circular (NOC) and relaxed (R) DNA. The DNA topoisomerase inhibitory activity of complex **1** was assayed in a concentration dependent manner with IC_{50} value of 30 μM.[33] As shown in Fig. 6, it was observed that the supercoiled DNA was converted to its nicked open circular form in the absence of complex **1**. However, upon increasing the concentration of complex **1**, the levels of the open circular form were inhibited (lanes 3–5). At 30 μM concentration (lane 6) of complex **1**, the DNA relaxation activity of Topo-I was significantly inhibited. These results revealed that complex **1** may block the DNA strand passage event of the enzyme and serve as catalytic inhibitors of Topo-I. Topo-I inhibition by **1** occurs either by (i) strong DNA binding and thereby preventing the binding of Topo-I to DNA and exercising its function, or (ii) binding to Topo-I and inactivating its proper functioning or (iii) stabilizing the catalytic topoisomerase I–DNA intermediate ('cleavable complex').

Superoxide dismutase activity. Superoxide dismutase (SOD) is one of the crucial essential enzymes that eliminates superoxide radical ($O_2^{\cdot -}$) and thus protects cells from damage induced by free radicals. The active $O_2^{\cdot -}$ production and low SOD activity in cancer cells may render the malignant cells since they are highly dependent on SOD for survival and sensitive to inhibition of SOD.[34] This critical function makes SOD an attractive target for pharmacological intervention. Therefore, it was interesting to investigate the SOD-like activity of complex **1** by using xanthine/xanthine oxidase assay due to their contributive solubility. SOD activity was monitored by reduction of nitro blue tetrazolium (NBT) with $O_2^{\cdot -}$ generated by xanthine/xanthine oxidase system. A plot of NBT percent inhibition with an increase in concentration of complex **1** is shown in Fig. 5. In addition, to ascertaining the effectiveness of the present complexes as functional SOD mimics, we compared the IC_{50} of several anti-inflammatory drug complexes (Fig. 7) which were previously determined using the NBT

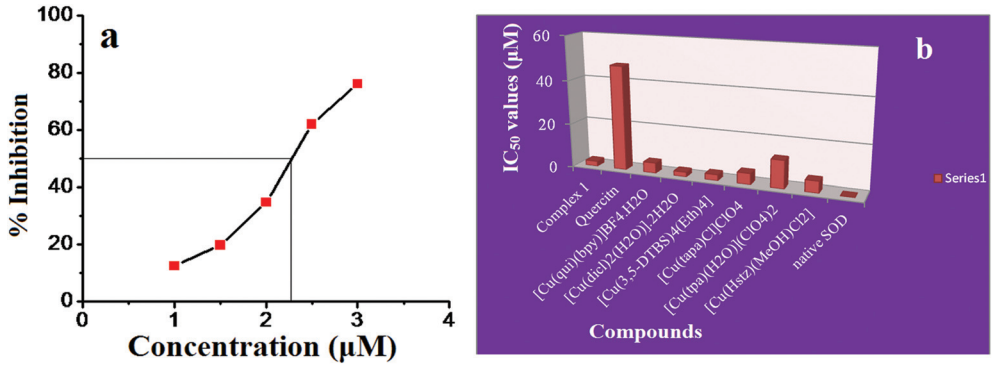

Fig. 7 (a) A plot of percentage of NBT inhibition reduction with an increase in the concentration of complex **1**. (b) Comparative IC_{50} values of complex **1** with quercetin and other monometallic copper complexes.

Table 1 SOD activities (IC_{50} values) of Cu^{II} complexes and native Cu_2,Zn_2-SOD

Compounds	IC_{50}	Ref.
Complex **1**	2.26	This work
Quercetin (ligand)	47.38	35
$[Cu(qui)(bpy)]BF_4{\cdot}H_2O$[a]	4.70	36
$[Cu(dicl)_2{\cdot}(H_2O)]{\cdot}2H_2O$[b]	2.13	37
$[Cu(3,5\text{-}DTBS)_4(Eth)_4]$[c]	2.69	37
$[Cu(tapa)Cl]ClO_4$[d]	5.02	38
$[Cu(tpa)(H_2O)](ClO_4)_2$[e]	12.50	38
$[Cu(Hstz)(EtOH)Cl_2]$[f]	5.170	39
Native Cu_2,Zn_2-SOD	0.04	39

[a] qui = 2-phenyl-3-hydroxy-4(1*H*)-quinolinone, bpy = 2,2′ bipyridine. [b] dicl = diclofenac acid. [c] 3,5-DTBS = 3,5-di-*tert*-butylsalicylate, Eth = ethanol. [d] tapa = tris(6-amino-2-pyridylmethyl)amine. [e] tpa = tris(2-pyridylmethyl)amine. [f] Hstz = protonated form of sulfathiazole.

method under the same conditions (Table 1).[35–39] The IC_{50} values obtained for complex **1** indicated that their SOD activity lies in the high activity region of the spectrum exhibited by copper complexes. The relatively high SOD mimic activity exhibited by complex **1** may be attributed to a significant contribution of the C_2–C_3 double bond and 3′,4′ hydroxyl groups on the B-ring of the quercetin.[40] The reaction involves a Cu^{II} ion at the active site of enzyme E which causes dismutation of superoxide anions by redox cycling of Cu^{II} ions (Scheme 2). A free radical such as $O_2^{\cdot -}$ binds to Cu^{II} ion and transfers the electron which leads to a reduction of Cu^{II} ion to Cu^{I}. In the second step, this electron is passed from the Cu^{I} ion back to another superoxide anion which then combines with two protons to make hydrogen peroxide (H_2O_2).

$$E\text{-}Cu^{2+} + O_2^{\bullet -} \longrightarrow E\text{-}Cu^{+} + O_2$$

$$E\text{-}Cu^{+} + O_2^{\bullet -} + 2H^{+} \longrightarrow E\text{-}Cu^{2+} + H_2O_2$$

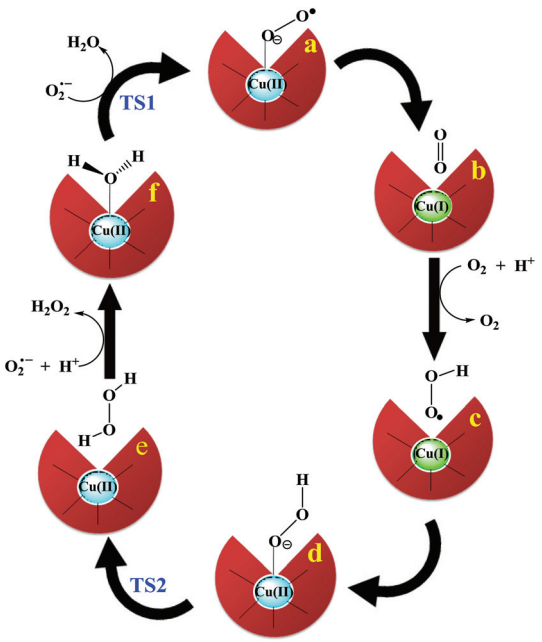

Scheme 2 Oxidation–reduction pathway during catalytic cycle of Cu–Zn SOD.

Therefore the π-electrons and hydroxyl groups of coordinated ligands may assist and stabilize the axial coordination of the $O_2^{\cdot -}$ anion to copper atom through hydrogen bond formation and electron transfer thereby giving rise to better SOD mimics.[41]

Molecular docking

The molecular docking technique is an attractive scaffold to understand the drug–macromolecular interactions for modern drug design and discovery and to predict the exact binding sites available at the molecular target such as DNA and enzymes. These docking programs, when used prior to experimental screening, can be considered as powerful computational filters in order to provide reliable information on the capability of new chemical entities to interact with DNA allowing us to quickly select the more interesting derivatives in a series of congeners.

Docking with DNA

To study the molecular basis of interaction mode and affinity of binding, complexes **1** and **2** were docked into DNA duplex of sequence $d(CGCGAATTCGCG)_2$ dodecamer (PDB ID: 1BNA) to search the proper binding site along with preferred orientation of the ligand inside the DNA minor groove. The complexes **1** and **2** adopted a characteristic crescent shape and were flexible enough to adopt a conformation complementary to the minor groove. It is well known that the interactions of chemical species with the minor groove of B-DNA differ from those occurring in the major groove, both in terms of electrostatic potential and steric-hindrance, because of the narrow shape of the former. In contrast to major groove, small molecules preferentially interact with the minor groove due to little steric interference.[42] In particular, the aromatic moieties of the DNA base pairs assumed a more planar conformation with respect to the ligands, compatible with stronger π–π stacking interactions and an overall better match of the ligands inside the DNA strands. The resulting docked pose (Fig. 8a and b),

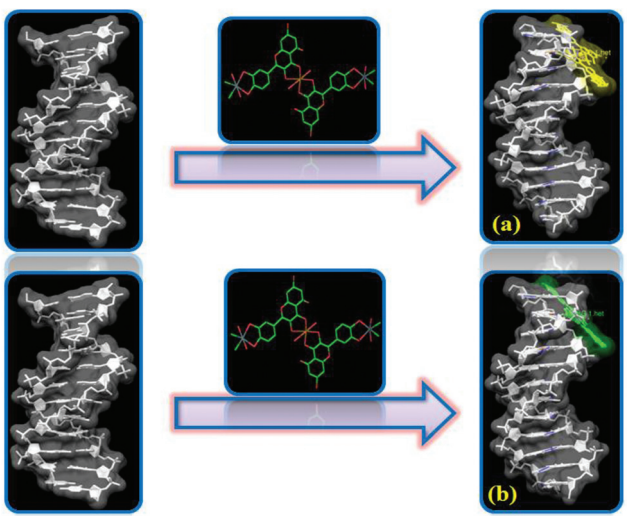

Fig. 8 Molecular docked model of complex (a) **1** and (b) **2** with DNA [dodecamer duplex of sequence $d(CGCGAATTCGCG)_2$ (PDB ID: 1BNA)].

revealed that the complexes bind to the narrow minor groove region of DNA within the G-C rich region and were stabilized by hydrogen bonding (2.8–3.0 Å) between the –OH groups of quercetin with O4/N2 atoms of C8/G8 bases in DNA. This indicates that it is possible to achieve sequence-selective binding. Moreover, changes in accessible surface area of interacting residues showed preferential binding of complexes towards the minor groove, and bends the DNA slightly in such a way that a part of the aromatic moiety of the quercetin ring could make favorable stacking interactions between the ring systems of the DNA bases, and lead to van der Waals interactions and hydrophobic contacts with DNA functional groups that define the stability of the groove.[43] The resulting relative binding energy of docked complexes **1** and **2** with DNA were found to be −287.6 and −241.2 eV, respectively, which is consistent with the binding affinity obtained from spectroscopic results is that complex **1** is more a prominent DNA binder than **2**.

Molecular docking with topoisomerase I

In order to verify the observed Topo-I inhibitory assay with complex **1**, molecular docking studies was performed with human-DNA–Topo-I complex (PDB ID: 1SC7) as illustrated in Fig. 9. The X-ray crystallographic structure of the human-DNA–Topo-I cleavable complex was retrieved from Protein Data Bank in which Topo-I is bound to the oligonucleotide sequence 5′-AAAAAGACTTsX-GAAAATTTTT-3′, where 's' is 5′-bridging phosphorothiolate of the cleaved strand and 'X' represents any of the four bases A, G, C or T. The phosphoester bond of G12 in 1SC7 was rebuilt and SH of G11 on the scissile strand was changed to OH (Fig. 9a).[44] The resulting docked model exhibited a dual binding mode of action on the activity of Topo-I due to bioactive conformation (related to structural flexibility) of the interacting quercetin molecule as well as a hydrogen bond accepting moiety. As shown in Fig. 9b, the planar quercetin aromatic system of rings **A** and **C** of complex **1** approaching towards the DNA cleavage site in the Topo-I–DNA complex and forming a stable complex through π–π stacking interactions between the G11 (+1; downstream) and pyrimidine ring of T10 (−1; upstream) whereas ring B protrude out of the helix interior into the minor groove and/or Topo-I functionalities on the scissile strand and C112 and A113, on the non-scissile strand, parallel to the plane of base pairs. Moreover, OH groups of quercetin probably involved in hydrogen bonding to Arg 364 residue, which is considered an essential amino acid that interacts with the ligand in the DNA–Topo-I active site. On the other hand, water-mediated H-bond interaction with the oxygen atom of G11 ribofuranose in the scissile strand, which could strongly block the rewinding step of the phosphoester, subsequently leading to inhibitory effect on Topo-I.[45] Furthermore, DNA intercalating forces were much more important than hydrogen bonding of the ligand to the surrounding amino acids residues of the protein, or to the base pairs.[46] Our molecular docking study proved the importance of DNA intercalating ability of **1** as well as H-bonding with the enzyme in the cleavage site. This result suggests that blocking the relegation of the G11 hydroxyl group could be the main point for novel Topo-I inhibitors. The model might serve as a rational basis for possible design of novel anticancer drugs targeting Topo-I.

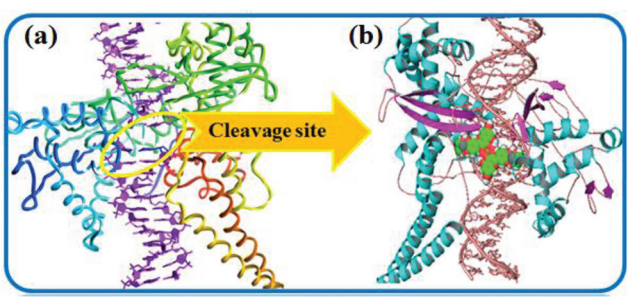

Fig. 9 Diagram showing in (a) human-DNA–Topo-I (70 kDa) (PDB ID: 1SC7) (b) molecular docked model of complex **1** in the cleavage active site of human DNA topoisomerase I (PDB ID: 1SC7).

Molecular docking with superoxide dismutase

To determine the mechanistic basis for the inhibitory action on SOD, complex **1** was successively docked towards the target active-site of bovine erythrocyte Cu, Zn superoxide dismutase (PDB ID: 2SOD). The crystal structure of the enzyme was obtained as 2 Å, resolution, and it revealed details of the active site; Cu^{II} and Zn^{II} lie 6.3 Å apart at the bottom of this long channel. The copper, which is essential for enzymatic activity, is surrounded by His-44, His-46, His-61 and His-118 and a weakly bound water molecule which occupies the axial position of a distorted square pyramid and is directed toward the cavity opening. However, zinc ion is surrounded by His-61, His-69, His-78 and Asp-81 and they are arranged in a tetrahedral structure and it is completely buried in the protein, and plays a key structural role in maintaining active site structural integrity during the catalytic cycle.[47,48] The side-chain of His61 forms a bridge between the Cu and Zn and is coplanar with them (Fig. 10a and b). Active sites are usually hydrophobic pockets that involve side chain atoms tightly packed;[49] thus we searched for these sites on the molecule surface by filtering out sites with significant convex surfaces too exposed to solvent. Since the only access to the copper ion is from the active-site cavity, the strong positive charge of the metal ions, along with two nearby positively-charged amino acids serve to draw the negatively-charged superoxide into the channel. Therefore, this interaction would be facilitated by the positive residues lining the channel such as Arg141, Lys120 and Lys134. The resulting docked model (Fig. 11) clearly indicated that the cationic core of the second metal ion Sn^{IV} surrounded by chlorine atoms can coordinate to the active-site copper as well as guanidyl cation of Arg141 and positively charged ammonia of Lys134 amino acid residues surrounding the active redox centre of SOD (*i.e.*, the Cu^{II}). Furthermore, the concentration of positive electrostatic potential) around the channel should facilitate the binding of anionic ligands in the cavity. This means the design of small molecular complexes to mimic the structure and functionality of SOD may be a

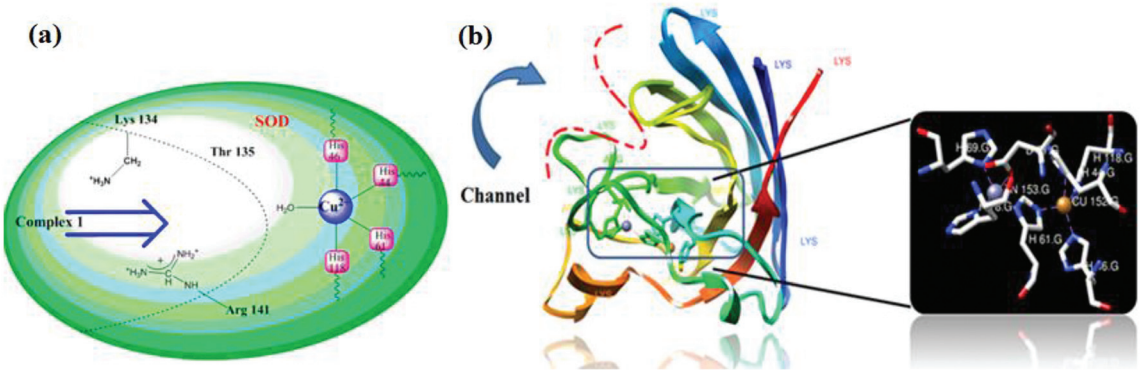

Fig. 10 (a) Schematic representation of the key–lock interaction between the CuZnSOD enzyme (PDB ID: 2SOD) and the complex **1**. (b) The active centre of CuZnSOD, taken directly from the X-ray structure for the enzyme. The copper ion is coloured red and the zinc ion coloured blue.

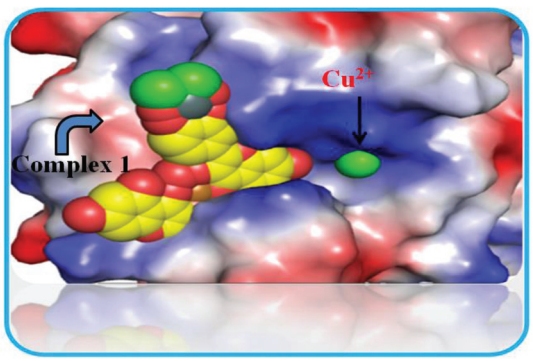

Fig. 11 Binding pose of complex **1** into the active-site channel of CuZnSOD enzyme. Arg141 and Thr135 act as a "bottleneck" for the active site, limiting the access of bulky anions to the copper shown as a green sphere at the bottom of the active-site channel.

promising approach to selectively killing cancer cells, and also mechanism-based combinations of SOD inhibitors.

Antitumor activity assays

The positive results obtained from the biological studies, namely, DNA binding, cleavage and Topo-I inhibition for complexes **1** and **2**, encouraged us to test their *in vitro* cytotoxic activity. The activity of complexes was evaluated in terms of GI_{50}, TGI and LC_{50} (Table 2) values against different human carcinoma cell lines of different histological origin: U373MG (CNS), PC3 (Prostate), Hop62 (Lung), HL60 (Leukemia), HCT15 (Colon), A2780 (Ovarian) and HeLa (Cervix) (Table S2†). The *in vitro* anti-tumor screening was evaluated by applying micro-culture Sulforhodamine B test (SRB)[50] and results revealed that complex **1** is more cytotoxic than that of the corresponding complex **2** against various human cancer cell lines, with a potency similar to that of the anticancer drug adriamycin (Fig. 12). These results showed the high potential of complex **1** to act as a drug candidate, as expected from the *in vitro* DNA binding studies and topoisomerase I catalytic inhibition. Among both the complexes, **1** exhibited very promising anti-tumor activity (GI_{50} < 10 μg ml^{-1}) against all these human carcinoma cell lines, indicating that it has the potential to act as an efficacious metal-based anticancer drug.

Experimental section

Reagents and materials

All reagents were commercially available and used as supplied without further purification. Copper nitrate trihydrate (Merck),

Table 2 Summary of the screening data of complexes **1** and **2** for the *in vitro* anti-tumor activity (in μM)

Human tissue of origin		CNS	Prostate	Lung	Leukemia	Colon	Ovarian	Cervix
Cell line		U373MG	PC3	Hop62	HL60	HCT15	A2780	HeLa
GI_{50}	**1**	<8.7	<8.7	<8.7	<8.7	<8.7	>69.6	<8.7
	2	42.5	40.0	36.5	31.9	42.8	41.1	7.7
	ADR	<17.2	<17.2	<17.2	<17.2	<17.2	56.0	<17.2
TGI	**1**	9.8	14.2	18.6	55.3	11.4	>137.9	<8.7
	2	>69.4	>69.4	>69.4	>69.4	>69.4	>69.4	44.4
	ADR	48.7	18.1	65.6	107.4	56.3	134.3	<17.2
LC_{50}	**1**	42.8	49.6	51.5	>69.6	45.8	>69.6	36.4
	2	>69.4	>69.4	>69.4	>69.4	>69.4	>69.4	>69.4
	ADR	116.7	85.68	>137.9	>137.9	>137.9	>137.9	>137.9

Note: GI_{50} = growth inhibition of 50% (GI_{50}) calculated from [(Ti − Tz)/(C − Tz)] × 100 = 50, drug concentration result in a 50% reduction in the net protein increase. ADR = adriamycin (taken as positive control compound). GI_{50} value <8.7 μM is considered to demonstrate activity. TGI = tumor growth inhibition. LC_{50} = lethal concentration of 50% (LC_{50}).

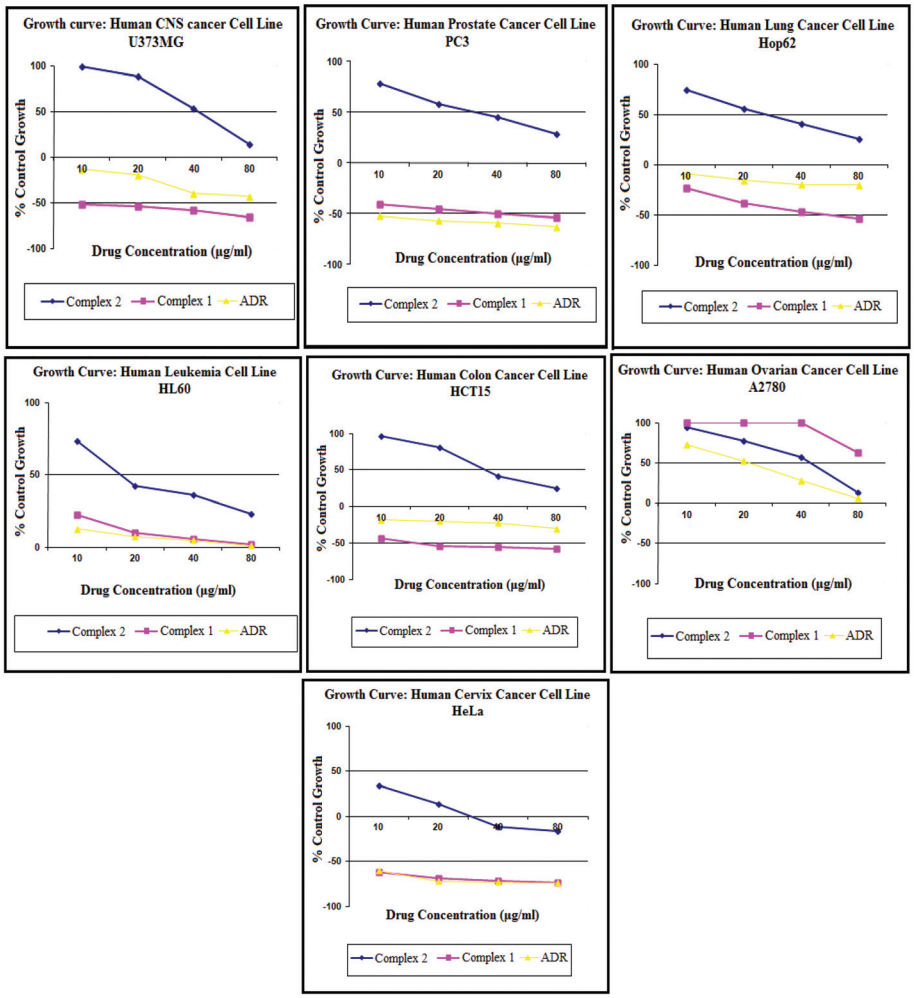

Fig. 12 Growth curve showing % control growth *verses* drug concentration (µg ml^{-1}) against different human carcinoma cell lines: U373MG (CNS), PC3 (Prostate), Hop62 (Lung), HL60 (Leukemia), HCT15 (Colon), A2780 (Ovarian) and HeLa (Cervix).

zinc nitrate hexahydrate, quercetin (Sigma-Aldrich), tin tetrachloride and calf thymus DNA (CT DNA). Human DNA topoisomerase I (Calbiochem), 6× loading dye (Fermental Life Science) and Supercoiled plasmid DNA pBR322 (Genei) were utilized as received.

Methods and instrumentation

Carbon, hydrogen and nitrogen contents were determined on Carlo Erba Analyser Model 1106. Molar conductance was measured at room temperature on CON 510 Bench conductivity TDS Meter. IR spectrum was recorded on Interspec 2020 FTIR spectrometer in KBr pellets from 400–4000 cm^{-1}. The ^{1}H, ^{13}C and ^{119}Sn NMR spectra were obtained on a Bruker DRX-400 spectrometer operating at room temperature. Electrospray mass spectra were recorded on Micromass Quattro II mass spectrometer. The TGA analysis of complexes was performed on Schimadzu DTG-60H analyzer under nitrogen atmosphere from room temperature to 1000 °C at a heating rate of 20 °C min^{-1}. The EPR spectrum of the copper complex was acquired on a Varian E 112 ESR spectrometer using X-band frequency (9.5 GHz) at liquid nitrogen temperature in liquid state. Electronic spectrum was recorded on UV-1700 PharmaSpec UV-vis spectrophotometer (Shimadzu) in DMSO cuvettes of 1 cm path length. Data were reported in λ_{max}/nm. Fluorescence measurements were determined on a RF-5301 PC spectrofluorophotometer (Schimadzu).

Synthesis of monometallic complexes $[Cu(Que)_2(H_2O)_2]$ and $[Zn(Que)_2(H_2O)_2]$

Monometallic complexes was synthesized by using $Cu(NO_3)_2 \cdot 6H_2O$ (0.241 g, 1 mmol)/$Zn(NO_3)_2$ (0.297 g, 1 mmol) and quercetin (0.604 g, 2 mmol) according to the procedure reported earlier.[51]

Synthesis of heterobimetallic complex $[Cu(Que)_2(H_2O)_6\text{-}Sn_2Cl_4]$ (1). To a methanolic solution of monometallic complex $[Cu(Que)_2(H_2O)_2]$ (0.70 g, 1 mmol), $SnCl_4$ (0.35 g, 2 mmol) was added dropwise. The resulting dark brown color solution obtained was refluxed for 6 h and was reduced to 5 ml by rotator evaporator. A brown color precipitate was obtained by adding ether to the above concentrated solution.

The complex obtained was filtered, washed with ether and dried *in vacuo*. Yield: 70%, m.p. > 300 °C (decompose). Analysis calculated for $C_{30}H_{26}Cl_4CuO_{20}Sn_2$ (%): C, 31.35; H, 2.28. Found: C, 31.40; H, 2.10. IR (KBr, ν_{max}/cm^{-1}): 3392 ν(O–H), 1620 ν(C=O), 1274 ν(C–O–C), 655 ν(Cu–O) and 416 ν(Sn–O). Molar conductance: Λ_M (1×10^{-3} M, DMSO): 19 Ω^{-1} cm^2 mol^{-1} (non-electrolyte). UV-vis absorption: λ_{max} (DMSO, 10^{-3} M), nm ($\varepsilon/10^3$ M^{-1} cm^{-1}) 275 (0.8), 430 (0.7) and 797 (0.5). ESI-MS (*m*/*z*, DMSO): 1113.6 $[C_{30}H_{26}Cl_4CuO_{20}Sn_2\text{-}2H_2O]^+$.

Synthesis of heterobimetallic complex $[Zn(Que)_2(H_2O)_6\text{-}Sn_2Cl_4]$ (2). This complex was synthesized with monometallic complex $[Zn(Que)_2(H_2O)_2]$ (0.70 g, 1 mmol) according to the procedure mentioned above. Yield: 60%, m.p. > 300 °C (decompose). Analysis calculated for $C_{30}H_{26}Cl_4O_{20}Sn_2Zn$ (%): C, 31.30; H, 2.28. Found: C, 31.24; H, 2.14. IR (KBr, ν_{max}/cm^{-1}): 3463 ν(O–H), 1644 ν(C=O), 1270 ν(C–O–C), 651 ν(Cu–O) and 404 ν(Sn–O). Molar conductance: Λ_M (1×10^{-3} M, DMSO): 28 Ω^{-1} cm^2 mol^{-1} (non-electrolyte). ^{1}H NMR δ_H (400 MHz; DMSO-d_6 ppm): 12.59 (5-OH), 10.68 (7-OH), 7.43 (2′-H), 7.13 (6′-H), 6.95 (5′-H), 6.56 (8-H) and 6.24 (6-H). ^{13}C NMR δ_C (100 MHz; DMSO-d_6 ppm): 175.6 (C=O), 164.2 (C-7), 160.8 (C-5), 158.8 (C-3′), 161.9 (C-4′), 155.8 (C-9), 146.8 (C-2), 139.4 (C-3), 133.1 (C-1′), 128.3 (C-5′), 127.2 (C-2′), 127.6 (C-6′), 124.2 (C-6), 122.6 (C-10) and 118.3 (C-8). ^{119}Sn NMR δ_{sn} (146 MHz; DMSO-d_6, ppm): −541.8 and −546.2. UV-vis absorption: λ_{max} (DMSO, 10^{-3} M), nm ($\varepsilon/10^3$ M^{-1} cm^{-1}) 273 (1.2) and 462 (0.8). ESI-MS (*m*/*z*, DMSO): 1115.5 $[C_{30}H_{26}Cl_4O_{20}Sn_2Zn\text{-}2H_2O]^+$.

DNA binding and cleavage experiments

DNA binding experiments including absorption spectral traces and emission spectroscopy conformed to the standard methods and practices previously adopted by our laboratory whereas the DNA cleavage experiment has been performed by the standard protocol.[52–55] While measuring the absorption spectra an equal amount of DNA was added to both the compound solution and the reference solution to eliminate the absorbance of the CT DNA itself, and Tris buffer was subtracted through base line correction.

Topoisomerase I inhibition assay

One unit of the enzyme was defined as completely relaxed 1 μg of negatively supercoiled pBR322 DNA in 30 min at 310 K under the standard assay conditions. The reaction mixture (30 μL) contained 35 mM Tris-HCl (pH 8.0), 72 mM KCl, 5 mM $MgCl_2$, 5 mM DTT, 2 mM spermidine, 0.1 mg ml^{-1} BSA, 0.25 μg pBR322 DNA, 2 Unit Topo-I and complex **1**. These reaction mixtures were incubated at 310 K for 30 min, and the reaction was terminated by addition of 4 μL of 5X buffer solution consisting of 0.25% bromophenol blue, 4.5% SDS and 45% glycerol. The samples were electrophoresed through 1% agarose in TAE at 30 V for 8 h.

Determination of the superoxide dismutase activity

Superoxide dismutase activity of complex **1** was assayed by using its ability to inhibit the reduction of nitroblue tetrazolium, NBT, at 560 nm by superoxide ions produced by the xanthine–xanthine oxidase system.[56–58] The assay was carried out in the assay buffer containing 50 mM Tris-HCl, pH 8.0, 0.1 mM diethylene triamine penta acetic acid (DTPA) and 0.1 mM hypoxanthine. The radical detector consists of a tetrazolium salt and is diluted by assay buffer. Similarly, the solutions of SOD standards and xanthine oxidase were prepared in sample buffer consisting of 50 mM Tris-HCl, pH 8.0. The SOD mimetic activity of the tested copper complex in aqueous solution at 25 °C was evaluated from the absorbance decrease at 560 nm comparing to the blank (the reaction mixture without the copper complex). The concentration of complex required to yield 50% inhibition of NBT reduction (the IC_{50} value) was determined from a plot of percentage inhibition *versus* complex concentration (μM).

Molecular docking

The rigid molecular docking studies were performed by using HEX 6.1 software,[59] which is an interactive molecular graphics program for calculating and displaying feasible docking modes of a pairs of protein, enzymes and DNA molecule. Structures of the complexes were sketched by CHEMSKETCH (http://www.acdlabs.com) and convert it into pdb format from mol format by OPENBABEL (http://www.vcclab.org/lab/babel/). The crystal structure of the B-DNA dodecamer d $(CGCGAATTCGCG)_2$ (PDB ID: 1BNA), native SOD (PDB ID: 1SXA) and human-DNA–Topo I complex (PDB ID: 1SC7) were downloaded from the protein data bank (http://www.rcsb.org./pdb). The minimization of the energy of the interacting complexes and receptor (DNA and enzyme) was performed by Ammp molecular dynamics software implementation of the VEGA OpenGL package version VEGA ZZ 2.4.0 using the SP4 force-field.[60] All calculations were carried out on an Intel pentium4, 2.4 GHz based machine running MS Windows XP SP2 as operating system. Visualization of the docked pose have been performed by using CHIMERA (http://www.cgl.ucsf.edu/chimera/) and PyMol (http://pymol.sourceforget.net/) molecular graphics program. The parameters used for the docking process *via* HEX docking Software were

- Correlation type – shape only
- FFT mode – 3D
- Grid dimension – 0.6
- Receptor range – 180
- Ligand range – 180
- Twist range – 360
- Distance range – 40

Antitumor activity assays

The following cell lines were used for *in vitro* antitumor screening; U373MG (CNS), PC3 (Prostate), Hop62 (Lung), HL60 (Leukemia), HCT15 (Colon), A2780 (Ovarian) and HeLa (Cervix). Human malignant cell lines were procured and grown in RPMI-1640 medium supplemented with 10% Fetal Bovine Serum (FBS) and antibiotics to study growth pattern of these cells. The proliferation of the cells upon treatment with chemotherapy was determined by means of the Sulphorhodamine-B (SR-B) semi-automated assay. All cell lines were seeded

into 96 well plates and cells were counted and the cell count was adjusted according to the titration readings so as to give optical density in the linear range (from 0.5 to 1.8) and were incubated at 37 °C in CO_2 incubator for 24 h. The stock solution of the complexes were prepared as 100 mg ml^{-1} in DMSO and four dilutions *i.e.* 10 μL, 20 μL, 40 μL, 80 μL, in triplicate were tested, each well receiving 90 μL of cell suspension. The plates were labeled properly and were incubated for 48 h. Termination of the experiment was carried out by gently layering the cells with 50 μL of chilled 30% TCA (in the case of adherent cells) and 50% TCA (in the case of suspension cell lines) for cell fixation and kept at 4 °C for 1 h. Plates stained with 50 μL of 0.4% SRB for 20 min. All experiments were made in triplicate.

Conclusion

In this work we have synthesized and characterized new heterobimetallic quercetin–Cu^{II}/Zn^{II}–Sn_2^{IV} complexes by using various spectroscopic and analytical methods. *In vitro* DNA binding studies of complexes **1** and **2** revealed the electrostatic mode of binding preferentially towards the oxygen atoms of the phosphate backbone reinstated further by coordinate covalent binding of Cu^{II}/Zn^{II} ion to N7/N3 atom of nucleobases. The complex **1** displayed efficient DNA groove binding propensity and cleavage activity through an oxidative mechanism induced by reactive oxygen species (ROS) while complex **2** follows the hydrolytic cleavage pathway. Furthermore complex **1** exhibited significant inhibitory effect on the catalytic activity of topoisomerase I at a low concentration of 30 μM. In addition complex **1** exhibited remarkable catalytic activity towards the dismutation of the superoxide anion with IC_{50} value of 2.26 μM. Therefore complex **1** acts as a potent SOD mimic with a good potential to be used for therapeutic application.

Acknowledgements

The authors are thankful to Sophisticated Analytical Instrumentation Facility, Panjab University, Chandigarh, for NMR and ESI-Mass facility; STIC, Cochin, for providing the elemental analysis; IIT, Bombay, for EPR measurements and ACTREC Mumbai, India for *in vitro* anticancer activity. We are also thankful to Department of Chemistry, Aligarh Muslim University for providing the TGA and FT-IR facility, DST-PURSE programme and DRS-1 (SAP) from UGC, New Delhi, India for their financial support. Author (Mehvash Zaki) are also highly grateful to CSIR-HRDG (SRF scheme-2013: 9/112(503) 2K13-EMR-I), New Delhi for providing financial assistance to promote my research work.

References

1 B. Rosenberg, *Interdiscip. Sci. Rev.*, 1978, **3**, 134.
2 (*a*) L. R. Kelland, *Drugs*, 2000, **59**, 1; (*b*) J. Reedijk, *Proc. Natl. Acad. Sci. U. S. A.*, 2003, **100**, 3611.
3 (*a*) P. J. Sadler and Z. Guo, *Pure Appl. Chem.*, 1998, **70**, 863; (*b*) S. Tabassum, M. Zaki, F. Arjmand and I. Ahmad, *J. Photochem. Photobiol., B*, 2012, **114**, 108.
4 G. Zuber, J. C. Quada Jr. and S. M. Hecht, *J. Am. Chem. Soc.*, 1998, **120**, 9368.
5 S. M. Hecht, *J. Nat. Prod.*, 2000, **63**, 158.
6 P. Kalaivani, R. Prabhakaran, F. Dallemer, P. Poornima, E. Vaishnavi, E. Ramachandran, V. V. Padma, R. Renganathan and K. Natarajan, *Metallomics*, 2012, **4**, 101.
7 C. Metcalfe and J. A. Thomas, *Chem. Soc. Rev.*, 2003, **32**, 215.
8 A. Silvestri, G. Barone, G. Ruisi, M. T. L. Giudice and S. Tumminello, *J. Inorg. Biochem.*, 2004, **98**, 589.
9 M. Navarro, E. J. C. Fajardo, A. Sierralta, M. F. Mestre, P. S. D. Arrieche and E. Marchan, *J. Biol. Inorg. Chem.*, 2003, **8**, 401.
10 S. Tabassum, R. A. Khan, F. Arjmand, M. Aziz, A. S. Juvekar and S. M. Zingde, *Carbohydr. Res.*, 2011, **346**, 2886.
11 F. Arjmand, S. Parveen, M. Afzal, L. Toupet and T. B. Hadda, *Eur. J. Med. Chem.*, 2012, **49**, 141.
12 E. Middleton, K. Chithan and T. C. Theoharides, *Pharmacol. Rev.*, 2000, **52**, 673.
13 C. Bailly, *Curr. Med. Chem.*, 2000, **7**, 39.
14 J. Zhou, L. Wang, J. Wang and N. Tang, *Transition Met. Chem.*, 2001, **26**, 57.
15 R. F. V. de Souza and W. F. D. Giovani, *Spectrochim. Acta, Part A*, 2005, **61**, 1985.
16 G. Dehghan and Z. Khoshkam, *Food Chem.*, 2012, **131**, 422.
17 E. Canpolat and M. Kaya, *J. Coord. Chem.*, 2004, **57**, 25.
18 D. C. Burns, D. A. Ellis and R. E. March, *Magn. Reson. Chem.*, 2007, **45**, 835.
19 C. Pettinari, F. Marchetti, R. Pettinari, D. Martini, A. Drozdov and Sergei Troyanov, *Inorg. Chim. Acta*, 2001, **325**, 103.
20 S. Chandra and L. K. Gupta, *Transition Met. Chem.*, 2005, **30**, 630.
21 R. N. Patel, A. Singh, K. K. Shukla, D. K. Patel and V. P. Sondhiya, *Transition Met. Chem.*, 2010, **35**, 577.
22 S. B. Bukhari, S. Memon, M. M. Tahir and M. I. Bhanger, *J. Mol. Struct.*, 2008, **892**, 39.
23 S. K. Sahni, R. V. Bennekom and J. Reedijk, *Polyhedron*, 1985, **4**, 1643.
24 F. Arjmand and A. Jamsheera, *Spectrochim. Acta, Part A*, 2011, **78**, 45.
25 F. Arjmand and F. Sayeed, *J. Mol. Struct.*, 2010, **965**, 14.
26 F. Arjmand and M. Muddassir, *Chirality*, 2011, **23**, 250.
27 F. Arjmand and S. Parveen, *RSC Adv.*, 2012, **2**, 6354.
28 M. Chauhan, K. Banerjee and F. Arjmand, *Inorg. Chem.*, 2007, **46**, 3072.
29 F. Dimiza, A. N. Papadopoulos, V. Tangoulis, V. Psycharis, C. P. Raptopoulou, D. P. Kessissogloua and G. Psomas, *Dalton Trans.*, 2010, **39**, 4517.
30 P. Kumar, S. Gorai, M. K. Santra, B. Mondal and D. Manna, *Dalton Trans.*, 2012, **41**, 7573.
31 S. Tabassum, R. A. Khan, F. Arjmand, A. S. Juvekar and S. M. Zingde, *Eur. J. Med. Chem.*, 2010, **45**, 4797.

32 J. Tan, B. Wang and L. Zhu, *JBIC, J. Biol. Inorg. Chem.*, 2009, **14**, 727.
33 Y. Mizushina, T. Akihisa, M. Ukiya, C. Murakami, I. Kuriyama, X. Xu, H. Yoshida and K. Sakaguchi, *Cancer Sci.*, 2004, **95**, 354.
34 P. Huang, L. Feng, E. A. Oldham, M. J. Keating and W. Plunkett, *Nature*, 2000, **407**, 390.
35 B. Hazra, S. Biswas and N. Mandal, *BMC Complementary Altern. Med.*, 2008, **8**, 63.
36 R. Buchtik, Z. Travnicek and J. Vanco, *J. Inorg. Biochem.*, 2012, **116**, 163.
37 A. L. Abuhijleh and J. Khalaf, *Eur. J. Med. Chem.*, 2010, **45**, 3811.
38 K. Jitsukawa, M. Harata, H. Arii, H. Sakurai and H. Masuda, *Inorg. Chim. Acta*, 2001, **324**, 108.
39 J. E. Weder, C. T. Dillon, T. W. Hambley, B. J. Kennedy, P. A. Lay, J. R. Biffin, H. L. Regtop and N. M. Davies, *Coord. Chem. Rev.*, 2002, **232**, 95.
40 E. Middleton, JR, C. Kandaswami and T. C. Theoharides, *Pharmacol. Rev.*, 2000, **52**, 673.
41 S. J. S. Flora, *Oxid. Med. Cell. Longevity*, 2009, **2**(4), 191.
42 R. Corradini, S. Sforza, T. Tedeshi and R. Marchelli, *Chirality*, 2007, **19**, 269.
43 R. Filosa, A. Peduto, S. Di Micco, P. de Caprariis, M. Festa, A. Petrella, G. Capranico and G. Bifulco, *Bioorg. Med. Chem.*, 2009, **17**, 13.
44 X. Xiao, S. Antony, Y. Pommier and M. Cushman, *J. Med. Chem.*, 2005, **48**, 3231.
45 H. T. M. Van and W.-J. Cho, *Bioorg. Med. Chem. Lett.*, 2009, **19**, 2551.
46 X. Xiao and M. Cushman, *J. Am. Chem. Soc.*, 2005, **127**, 9960.
47 J. A. Tainer, E. D. Getzoff, K. M. Beem, J. S. Richardson and D. C. Richardson, *J. Mol. Biol.*, 1982, **160**, 181.
48 R. J.F. Branco, P. A. Fernandes and M. J. Ramos, *Theor. Chem. Acc.*, 2005, **115**, 27.
49 H. X. Zhou, K. Y. Wong and M. V. Kumar, *Proc. Natl. Acad. Sci. U. S. A.*, 1997, **94**, 12372.
50 T. Lammers, P. Peschke, V. Ehemann, J. Debus, B. Slobodin, S. Lavi and P. Huber, *Mol. Cancer*, 2007, **6**, 65.
51 (*a*) J. Zhou, L. F. Wang, J. Y. Wang and N. Tang, *Transition Met. Chem.*, 2001, **26**, 57; (*b*) J. Tan, L. Zhua and Bochu Wang, *Dalton Trans.*, 2009, 4722.
52 M. E. Reicmann, S. A. Rice, C. A. Thomas and P. Doty, *J. Am. Chem. Soc.*, 1954, **76**, 3047.
53 A. Wolfe, G. H. Shimer and T. Meehan, *Biochemistry*, 1987, **26**, 6392.
54 J. R. Lakowiez and G. Webber, *Biochemistry*, 1973, **12**, 4161.
55 F. Arjmand and M. Mudassir, *Eur. J. Med. Chem.*, 2010, **45**, 3549.
56 D. K. Demertzi, A. Galani, M. A. Demertzis, S. Skoulika, C. Kotoglou and J. Inorg, *Biochemistry*, 2004, **98**, 358.
57 A. L. Abuhijleh and C. Woods, *Inorg. Chem. Commun.*, 2002, **5**, 269.
58 G. Lupidi, F. Marchetti, N. Masciocchi, D. L. Reger, S. Tabassum, P. Astolfi, E. Damiani and C. Pettinari, *J. Inorg. Biochem.*, 2010, **104**, 820.
59 D. Mustard and D. W. Ritchie, *Proteins: Struct., Funct., Bioinf.*, 2005, **60**, 269.
60 A. Pedretti, L. Villa and G. Vistoli, *J. Mol. Graphics Modell.*, 2002, **21**, 47.